Temporal pixel multiplexing for simultaneous high-speed, high-resolution imaging

Gil Bub[1], Matthias Tecza[2], Michiel Helmes[1], Peter Lee[1] & Peter Kohl[1]

We introduce an imaging modality that, by offsetting pixel-exposure times during capture of a single image frame, embeds temporal information in each frame. This allows simultaneous acquisition of full-resolution images at native detector frame rates and high-speed image sequences at reduced resolution, without increasing bandwidth requirements. We demonstrate this method using macroscopic and microscopic examples, including imaging calcium transients in heart cells at 250 Hz using a 10-Hz megapixel camera.

Conventional cameras capture images at a fixed spatial and temporal resolution. Events that occur faster than the detector integration time (t_i) appear blurred (if moving), as an average light intensity (if changing intensity while stationary) or as a combination thereof. We propose a temporal pixel multiplexing (TPM) paradigm for imaging that allows simultaneous high-speed and high-resolution image capture on a single detector.

The method is based on subdividing a charge-coupled device (CCD) array into m nonoverlapping groups of n pixels (**Fig. 1** and **Supplementary Fig. 1**). Individual pixels in each group capture their part of the imaged scene sequentially so that at any instant, m spatially dispersed pixels are subsampling the image with an exposure duration $t_e = t_i \times n^{-1}$. As all detector pixels are exposed at some point during t_i, the resulting full frame image is qualitatively similar to that of a conventionally acquired high-resolution image (**Supplementary Fig. 2**). In addition, n subframes can be extracted from co-exposed pixels in all m groups. The spatial resolution of each subframe is n times lower than that of the full frame, but the image sequence has an n times higher temporal resolution than can be achieved using the conventional image-capture mode of the same detector. Thus, TPM embeds high-speed temporal information in an image while increasing neither memory requirements nor the intrinsic frame rate of the camera. Static regions of the high-resolution image are unchanged, and high-speed information is multiplexed into image regions that would normally appear blurred.

A principal design requirement is that cohorts of spatially distinct subregions of the imaging chip are sequentially exposed for periods t_e shorter than t_i of the camera. Subregion exposure control can be implemented on the illumination side, using patterned light techniques such as applied to superresolution[1] and confocal[2] imaging. Alternatively, light can be blocked on the detector side, as done in dynamic filtering[3] and single-pixel camera[4] applications. Finally, TPM could be incorporated into new complementary metal oxide semiconductor (CMOS) sensor designs by offsetting pixel sample and digitization times. Here we present a prototype that uses a digital micromirror device[5] (DMD) to transiently expose subregions of a CCD (Online Methods).

TPM functionality is illustrated in **Figure 2**. We captured a high-resolution image of a macroscopic scene using a 25 frames per second (fps) megapixel camera while the DMD cycled through a sequence of 16 mirror patterns during each full frame acquisition (t_i = 40 ms; t_e = 2.5 ms), yielding a final frame rate of the embedded lower-resolution image sequence of 400 fps (**Fig. 2b**). As all pixels were exposed during t_i, the unprocessed frame captured high-spatial-resolution details of the imaged scene. After extracting and combining simultaneously exposed pixels, the blurred regions in the high-resolution low-speed image were resolved as an image sequence of a drop of opaque liquid (milk) falling into a beaker filled with water (**Fig. 2b**, **Supplementary Fig. 3** and **Supplementary Video 1**).

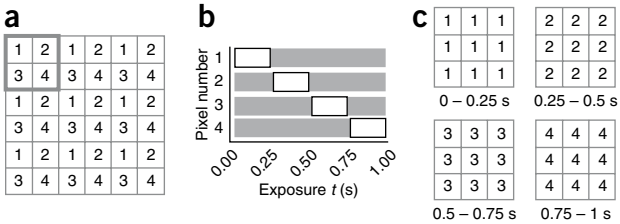

Figure 1 | Schematic of TPM principle. (**a**) A detector (6 × 6 pixels) with a frame rate of 1 fps is organized into m = 9 exposure groups, each consisting of n = 4 light-detecting elements (arranged in a 2 × 2 grid pattern; solid outline). Each numbered element corresponds to one pixel (in general, exposure elements can consist of multiple neighboring pixels). (**b**) Each pixel with the same identifier in all exposure groups integrates light at the same time, for a quarter of the detector's total exposure time (for $t_i \times n^{-1}$, here 0.25 s). The full-resolution frame is read out and digitized after 1 s. (**c**) A subframe is extracted from all pixels exposed over the first 0.25 s (consisting of all m pixels with identifier 1), a second subframe exposed from 0.25 to 0.5 s is extracted from all m pixels with identifier 2 and so on, to give four sequential 9-pixel frames, collected at 4 fps (n times the inherent full-frame rate). The full resolution frame is simultaneously obtained.

[1]Department of Physiology Anatomy and Genetics and [2]Department of Physics, University of Oxford, Oxford, UK. Correspondence should be addressed to G.B. (gil.bub@dpag.ox.ac.uk).

RECEIVED 23 OCTOBER 2009; ACCEPTED 4 JANUARY 2010; PUBLISHED ONLINE 14 FEBRUARY 2010; DOI:10.1038/NMETH.1429

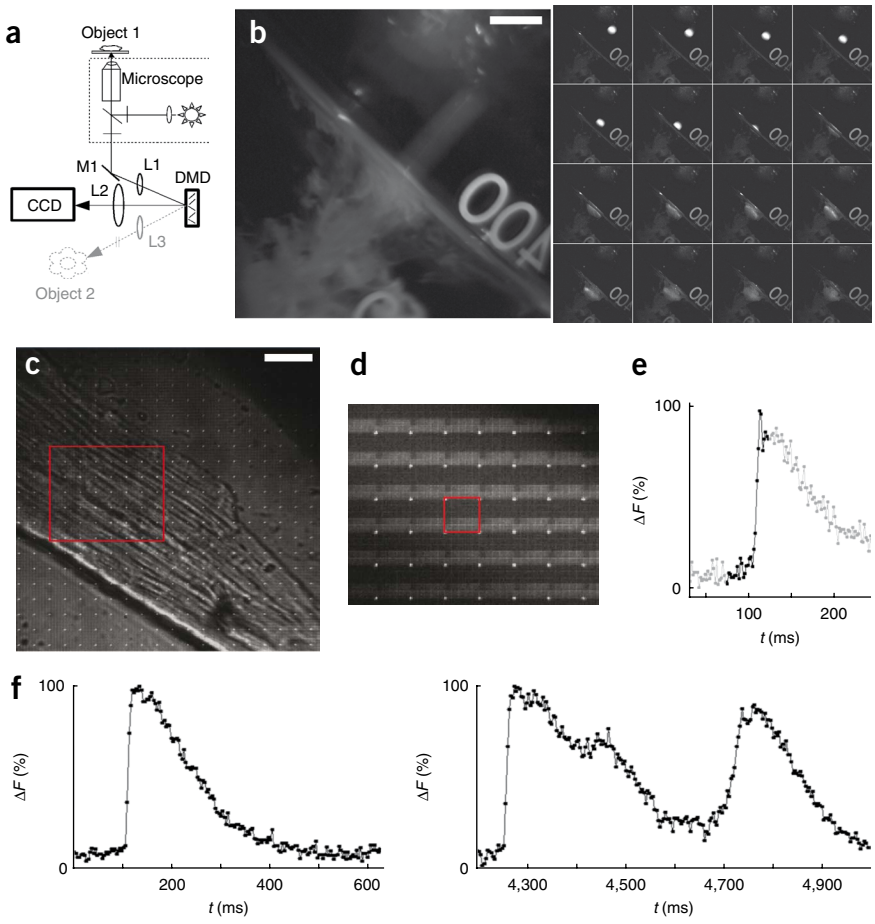

Figure 2 | Functional TPM prototype. (**a**) A diagram of the prototype, which can capture microscopic (black lines, via mirror (M1) and lens 1 (L1)) or macroscopic images (gray lines, via lens 3 (L3)). (**b**) High-resolution frame (left; 1,000 × 1,000 pixels, 25 fps) and 16 embedded high-speed subframes (right; 250 × 250 pixels, 400 fps) showing a milk drop falling into water, captured via lens 3. (**c**) Cardiac cell loaded with a calcium-sensitive dye, imaged with a megapixel camera at t_i = 100 ms. The DMD was programmed to sequentially expose a 5 × 5 pattern of exposure elements (where each element consisted of 25 neighboring pixels), for t_e = 4 ms. Bright points are mirrors toggled to the 'always on' position, for alignment purposes. (**d**) Close-up of the boxed region in **c** during an action potential, showing intensity changes mapped to detector location (after background frame subtraction, which removes visible structural detail). Every exposure group (such as the one outlined in red) measured fluorescence intensity from a 25 × 25 pixel area. (**e**) Intensity versus time plot for one of the exposure groups, extracted by sequentially plotting the intensity recorded by each of the 25 elements. Dark points correspond to pixel values in **d**; and gray points were extracted from frames before and after. (**f**) Average intensity values for all pixels in **d** resolve the whole-cell calcium transient shape with improved SNR. Analysis of the calcium dynamics showed that a normal beat was followed by one with an early and delayed after-contraction. Scale bars, 4 mm (**b**) and 6 μm (**c**).

The method is also useful for measuring intensity-coded processes, such as those encountered in functional imaging of cardiac[6] and neuronal[7] cell networks. Rapid ion-concentration and membrane-voltage changes can be mapped to light intensity using fluorescent probes. As high-resolution detectors suffer noise and bandwidth limitations at high frame rates, and as image intensification technology imposes dynamic range limitations[8,9], researchers typically rely on high-speed, high-dynamic-range, low-resolution detectors, ranging from 16 × 16 photodiode arrays[6] to specialized low resolution CCD[7] and CMOS[10] cameras. Additional high spatial resolution cameras are required to interrelate structure and function.

We conducted a proof-of-principle microscopic fluorescence mapping study in rat cardiac myocytes. We loaded cells with the calcium-sensitive dye Rhod-2 and imaged them at 40× using an inverted microscope. We captured high-resolution cell structure images (**Fig. 2c**,**d**) and simultaneously measured functional whole-cell calcium transients at high speed (**Fig. 2e**,**f**). The effective frame rate of calcium transient capture was more than an order of magnitude greater than that of the camera itself (250 fps versus 10 fps) and considerably exceeded the camera's maximum region-of-interest or on-chip binning frame rates. Furthermore, despite light losses caused by transient pixel exposure, the fluorescent signal-to-noise ratio (SNR) was high and equivalent to that of specialized high-speed, low-resolution devices, such as photodiode arrays, dedicated high-speed CCDs or photomultiplier tubes.

TPM is a contribution to advanced imaging techniques that embed information in images by modulating light. Lens arrays[11] and shaped apertures[12] are used to partially encode light fields in images, allowing users to change viewpoints or focal planes after acquisition. Patterned light has been used to embed three-dimensional information in images[13] and perform optical sections[2] in microscopy applications. High-speed motion has also been targeted: coded-exposure photography[14] embeds spatial frequency detail in images by globally modulating exposure during acquisition, allowing motion blur to be algorithmically corrected. However, coded exposure methods depend on a known and reproducible motion path, and as pixels are repeatedly exposed during each frame, intensity changes in stationary objects (such as cells) cannot be measured. In contrast, TPM exposes pixel subsets at discrete times using one detector, a strategy that has previously been implemented using multiple detectors in high-speed dense camera arrays[15].

TPM has several advantages over conventional high-speed imaging methods. Not only does it provide simultaneous high-resolution and high-speed datasets using just one detector, but data throughput requirements are the same as those of a single high-resolution image sequence. This allows slow-scan cameras with their known advantages in terms of cost, SNR and dynamic range[8,11] to be used for high-speed imaging tasks. The system is modular (it can be added to existing detectors) and highly flexible: our present implementation allows for nonrectangular regions of interest (pixel groups in the shape of cells, for example) and supports different frame rates for different areas of the CCD, which is not possible using conventional detectors.

METHODS

Methods and any associated references are available in the online version of the paper at http://www.nature.com/naturemethods/.

Note: Supplementary information is available on the Nature Methods website.

ACKNOWLEDGMENTS

We thank P. Cobden and R. Vaughan-Jones for providing isolated cells, A. Garny for help with editing, and Oxford University's Isis Innovation, the UK Biotechnology and Biological Sciences Research Council and the British Heart Foundation for financial support.

AUTHOR CONTRIBUTIONS

G.B. developed the original concept; G.B. and M.T. designed and built the apparatus; M.H., P.L. and P.K. gave technical and/or conceptual support; G.B. performed experiments; G.B. and P.K. wrote the paper.

COMPETING INTERESTS STATEMENT

The authors declare competing financial interests: details accompany the full-text HTML version of the paper at http://www.nature.com/naturemethods/.

Published online at http://www.nature.com/naturemethods/.
Reprints and permissions information is available online at http://npg.nature.com/reprintsandpermissions/.

1. Kner, P., Chhun, B.B., Griffis, E.R., Winoto, L. & Gustafsson, M.G.L. *Nat. Methods* **6**, 339–342 (2009).
2. Hanley, Q.S., Verveer, P.J., Gemkow, M.J., Arndt-Jovin, D. & Jovin, T.M. *J. Microsc.* **196**, 317–331 (1999).
3. Nayar, S.K., Branzoi, V. & Boult, T.E. *Int. J. Comput. Vis.* **70**, 7–22 (2006).
4. Takhar, D. *et al. Computational Imaging IV* **6065**, 43–52 (2006).
5. Hoefling, R. *Proc. SPIE* **5303**, 1117/12.528341 (2004).
6. Efimov, I.R., Nikolski, V.P. & Salama, G. *Circ. Res.* **95**, 21–33 (2004).
7. Spors, H., Wachowiak, M., Cohen, L.B. & Friedrich, R.W. *J. Neurosci.* **26**, 1247–1259 (2006).
8. Denvir, D. & Conroy, E. *Proc. SPIE* **4796**, 164–174 (2003).
9. Entcheva, E. & Bien, H. *Prog. Biophys. Mol. Biol.* **92**, 232–257 (2006).
10. Tallini, Y.N. *et al. Proc. Natl. Acad. Sci. USA* **103**, 4753–4758 (2006).
11. Tominaga, T., Tominaga, Y., Yamada, H., Matsumoto, G. & Ichikawa, M. *J. Neurosci. Methods* **102**, 11–23 (2000).
12. Levoy, M., Zhang, Z. & McDowall, I. *J. Microsc.* **235**, 144–162 (2009).
13. Veeraraghavan, A., Raskar, R., Agrawal, A., Mohan, A. & Tumblin, J. *ACM Trans. Graph.* **26**, 69:1–69:12 (2007).
14. Agrawal, A. & Raskar, R. *Proc. IEEE Comput. Soc. Conf. Comput. Vis. Pattern Recognit.* **2007**, 1–8 (2007).
15. Wilburn, B., Joshi, N., Vaish, V., Levoy, M. & Horowitz, M. *Proc. CVPR* **2004**, 294–301 (2004).

ONLINE METHODS

Cell isolation. Rat ventricular myocyte isolation has been described in detail elsewhere[16]. In short, hearts were initially Langendorff-perfused with a modified Tyrode solution containing 128 mM NaCl, 2.6 mM KCl, 2.0 mM $CaCl_2$, 1.18 mM $MgSO_4$, 1.18 mM KH_2PO_4, 10 mM HEPES, 20 mM taurine, 11 mM glucose and 5,000 units l^{-1} heparin (pH 7.4); followed by cardioplegic solution (20 mM K^+; no heparin or calcium) to induce cardiac arrest. Upon induction of arrest, the perfusate was changed for 12 min to enzyme-containing solution (0.24 mg ml^{-1} BlendZymes III; Roche). The tissue was then collected, minced and gently agitated in 10 ml enzymatic solution. This solution was collected every 5 min (5 repeats), filtered and centrifuged for 1 min at 18*g* (Precision Durafuge 100). The supernatant was discarded and the cell pellet was resuspended in cell culture medium (DMEM; Sigma). Cells were kept at room temperature (25 °C).

Calcium fluorescence. Cells were loaded with the calcium-sensitive dye Rhod-2 for 20 min (Rhod-2AM 5 mM; Invitrogen), washed in Tyrode solution and imaged after 10 min to allow for esterase-mediated dye cleavage. Dye-loaded cells were transferred to a glass-bottomed dish and imaged using an inverted microscope (Nikon Diaphot, 1.3 numerical aperture (NA) oil immersion lens) with a Rhod-2 fluorescence cube (Chroma, excitation 540/25 nm band pass, dichroic 565 nm, emission 605/655 nm band pass, excited with an Xe-Hg light source; Optiquip).

Optical path. The optical path was aligned so that an imaged scene was first focused on the DMD[17] array, which in turn was focused on the camera. The camera and mirror array were positioned to allow imaging from the side port of a microscope (Nikon Diaphot, 40× oil immersion lens), or for macroscopic imaging using a suitable projection lens (for example, lens 3 in **Fig. 2a**). In both cases, light was focused to form an image on the DMD array. Light from the microscope side port was directed to the DMD using a plane mirror to an achromatic lens pair (100 mm focal length; Thorlabs). The Texas Instruments XGA+ (1,400 × 1,050 mirror) DMD array (Vialux) was mounted in a custom housing that was attached on a 6-axis micropositioning stage (MAX312 and APY002 from Thorlabs, M-TGN120 from Newport) for alignment of mirrors with camera pixels. Light from the DMD was focused on a camera (GC1380H, Sony ICX285 sensor, 1,360 × 1,024 pixels, Prosilica) using a 100 mm SLR lens (f/2 Makro-Planar T* Zeiss) so that a single mirror was in register with each pixel in the CCD (excess DMD mirrors were not used for projection). For the experiments shown in **Figure 2**, the center 1,000 × 1,000 pixel per mirror pairs were used. The camera and lens were coupled using Thorlabs 30 and 60 mm cage components with a rotation mount for camera angle adjustment (Thorlabs CRM1P) and positioned using a linear stage (Newport M423). Additional optical configurations are discussed in a patent application (Bub, G., patent application PCT/EP2008/003702; 2008).

Alignment and synchronization. The camera and mirror array were aligned visually using custom software that allows live zoom display of 50 equidistant 10 × 10 mirror areas, each set so a single mirror was in the 'on' position, dispersed over the mirror array surface. Once aligned, the mirror array was set to repeatedly cycle through frame series of n mirror patterns, where each pattern is active for t_e ms. The camera was set to trigger off every n^{th} DMD pattern by setting the camera frame duration to $t_e \times n + t_r$, where t_r is the frame readout time. t_r is small (0.184 ms for the GC1380H) compared to camera integration time ($t_i = t_e \times n$) and has thus been ignored in the schematic description of TPM elsewhere. Frames were continually saved to hard disk for later analysis.

Exposure patterns. The mirror array can be programmed to cycle through a series of binary images, so that each mirror acts as a pixel level shutter that can open and close faster than the camera exposure time t_i. Individual mirrors were classified for programming purposes as being part of exposure elements, exposure groups and subframe elements (**Supplementary Fig. 4**). As mirrors were pixel-matched to the detector, a corresponding pattern was created on the image, and pixels and mirrors were functionally equivalent. Exposure elements (**Supplementary Fig. 4**) refer to locally adjacent mirrors that were programmed to have the same on/off state. Here each exposure element consisted of 4 mirrors (in contrast, in **Fig. 1**, each element corresponds to one mirror/one pixel). An exposure group consisted of a set of locally adjacent exposure elements that cycled through a sequence of on/off states, so that CCD pixels in register with mirrors in the exposure group collected light at different times during t_i. Mirrors in different exposure groups with the same identifier behaved identically. Simultaneously exposed pixels were termed subframe elements and could be extracted, conserving their spatial interrelation, to form a subframe (for example, pixels forming the seventh subframe are shown outlined in blue). In **Supplementary Figure 4**, a (hypothetical) 12 × 12 mirror array is organized into four exposure groups ($m = 4$), each containing nine 4-pixel exposure elements ($n = 9$). Each subframe consists of four spatially dispersed co-exposed four-pixel elements (with the same identifier) providing a temporal resolution that is $n = 9$ times better that the detector's intrinsic frame rate.

In addition to the sequential patterns (**Fig. 1** and **Supplementary Fig. 4**), exposure patterns could be randomized to reduce potential effects of regularly spaced exposure elements in the high-resolution image. Here each exposure group had the same dimension and number of exposure elements as before, but the exposure sequence of individual elements (with the same identifier) was shuffled using a random seed. This way, co-exposed elements did not display a periodic spatial pattern, and the high-resolution image appeared qualitatively more similar to a conventional image. High-resolution images captured using a conventional technique, periodic exposure patterns and randomized exposure patterns are compared in **Supplementary Figure 2a–c**.

For macroscopic scene imaging (**Fig. 2b**), the mirror array was divided into a grid pattern of 62,500 ($1{,}000{,}000 \times 16^{-1}$) exposure groups, each comprising 4 × 4 adjacent mirrors (here exposure element size = 1 pixel). Mirrors within each exposure group were programmed to reflect light to in-register pixels on the camera so that each pixel was exposed for 2.5 ms in a sequential fashion, and each 1,000 × 1,000 pixel frame was read out and stored after 40 ms.

For fluorescence imaging (**Fig. 2c–g**), the mirror array was divided into 1,600 exposure groups, each comprising 625 (25 × 25) adjacent mirrors. To improve contrast, mirrors were grouped into exposure elements of 25 (5 × 5) adjacent mirrors (pixels on

doi:10.1038/nmeth.1429

the detector). Each exposure group consisted of a 5 × 5 pattern of these multipixel elements. Each exposure element sequentially reflected light to 5 × 5 groups of in-register pixels for 4 ms, and each 1,000 × 1,000 pixel frame was read out and stored after 100 ms. The corner mirror in each exposure group was fixed to the 'on' position for some runs to aid alignment (**Fig. 2c**,**d**).

Postprocessing. Pixels exposed over the same interval were grouped in software to generate a higher-speed lower-resolution image sequence. As the mirror and pixel dimensions were small (13.68 μm^2 and 6.45 μm^2, respectively), and image focus can be suboptimal, pixels integrated stray light from adjacent regions. In practice, the maximum contrast ratio at the individual pixel level (ratio of pixel intensity to that of its nearest neighbor) was approximately 4. For macroscopic scene imaging, where each pixel cluster consisted of only one pixel, images were optionally sharpened before decoding with 3 × 3 Laplacian kernel.

For the fluorescence data shown in **Figure 2c–f**, sharpening was not used. Instead, the pixels along the border of each 5 × 5 pixel exposure element were discarded and the remaining pixel values with identical identifiers were averaged for each exposure element. Contrast ratio using this scheme was high (>1,000:1). Average cluster values were plotted as a function of time (4 ms intervals). To remove the effects of high spatial frequency structures on the analysis, the first high-resolution image was used as a background image, which was subtracted from each subsequent high-resolution image before extracting the high speed calcium fluorescence time series (compare background in **Fig. 2c** to that in **Fig. 2d**). The time series data in **Figure 2e**,**f** are unfiltered.

Image processing. High-resolution TMP images contain high spatial frequency components that can lead to visual artifacts if reproduced or viewed at less than full resolution. The full resolution image in **Figure 2b** was processed using a three pixel radius Gaussian blur to avoid these potential effects. The unaltered full 1,000 × 1,000 pixel image is available as **Supplementary Figure 3**.

Limitations. The method embeds high-speed information into static frames by transiently exposing pixels to light in a controlled fashion. As a consequence of this process, the majority of the light is deflected away from the sensor by the DMD. However, as each pixel collects light with high efficiency over its exposure period, signal quality can be high. Nonetheless, as light destined for neighboring elements in each exposure group is discarded for a fraction equivalent to $(n-1) \times n^{-1}$ of detector integration time, the method will be of low utility in highly light-limited situations where spatial pixel averaging (for example, adjacent pixel binning) may be required to obtain a high quality signal.

16. Yamamoto, T. *et al. J. Physiol. (Lond.)* **562**, 455–475 (2005).
17. Hofling, R. & Ahl, E. *Proc. SPIE* **2004**, 322–329 (2004).